The porcine atelocollagen layer was developed as follows [10]: the polypropylene framework was placed in a Teflon mould. Then, 1% collagen solution (Nippon Meat Packers, Inc., Osaka, Japan) was stirred at 8000 rpm for 15 min, and then poured into the space between the outer mould and the inner tube, and then freeze-dried. During this freeze-drying process, the cast collagen became a porous structure with a pore size range of 100 to 500×10^{-6} m. A 5-mm-thick collagen layer was formed on both internal and external luminal surfaces. Finally, the prosthesis was heated at 140°C under vacuum pressure for a 24-h dehydrothermal treatment session to induce moderate cross-linkage of the collagen molecules.

Animal experiments

Animal experiment 1. Development of a composite scaffold from polypropylene frameworks (in the omentum versus in the pouch of Douglas).

Five adult beagle dogs, weighing 8–14 kg, were anaesthetized with an intramuscular administration of 15 mg/kg ketamine hydrochloride and 7 mg/kg xylazine and then intubated with an endotracheal tube. Mechanical ventilation was maintained using inhalational sevoflurane. A 500-mg dose of ampicillin was injected intramuscularly prior to the skin incision. In each dog, a polypropylene framework was placed in the omental sac after making a slit on the omental peritoneum via an upper mid-line laparotomy (Fig. 2C), and another polypropylene framework was placed in the pouch of Douglas as a control (Fig. 2D). Both were extracted 3 weeks afterwards via a reoperative laparotomy. After sectioning each specimen into two transversely, the thickness of the developed connective tissue was measured with a ruler at three different points (every 120°) on the circumference.

Animal experiment 2. Development of a composite scaffold in the omentum (from polypropylene frameworks versus from polypropylene frameworks coated with a porcine atelocollagen layer).

Another five adult beagle dogs, weighing 8–14 kg, were anaesthesized in the same way as above. A 500-mg dose of ampicillin was injected intramuscularly prior to the skin incision. Two types of framework, as mentioned above, were both placed in the omental sac (Fig. 2E and F). Both were extracted 3 weeks afterwards as in Animal experiment 1, and the thickness of the developed connective tissue was measured in the same way.

All surgical procedures were performed by board-certified surgeons (Masatsugu Hamaji and Fumitsugu Kojima) in accordance with the Guide for the Care and Use of Laboratory Animals published by the National Institutes of Health (NIH Public-ation No. 85-23, revised 1985). The experimental protocol was approved by the Animal Experimental Committee of Kyoto University.

Following first laparotomies (for placement of polypropylene frameworks) or second laparotomies (for extraction of the frameworks), all the dogs received the same regular care as preoperatively. Macroscopic findings at reoperative laparotomies were obtained with a focus on developed connective tissue.

Radiological analysis of developing composite scaffolds

To follow-up the process of developing composite scaffolds in the omentum, four dogs were randomly selected from animal experiment 2 for abdominal computed tomography (CT). All CT images from the diaphragm to the hip joints were obtained with a 16-row multidetector CT scanner (Alexion 16, Toshiba Medical systems, Tochigi, Japan) with an intramuscular administration of ketamine and xylazine on postoperative day (POD) 0, 7, 14 and 21. The images were obtained in the helical mode with 120 kV voltage, 50 mA per section, a 512×512 matrix and 7-mm slice thickness. All images were interpreted by a board-certified radiologist (Sho Koyasu).

Histological analysis of developed connective tissue on the frameworks

In animal experiment 1, two scaffolds developed from polypropylene frameworks in the pouch of Doulgas and two scaffolds developed from polypropylene frameworks in the omentum (from two dogs) were sent for histological analysis by light microscopy after staining with haematoxylin and eosin (H&E), Masson trichrome (MT) and alpha-smooth muscle actin (α-SMA). The number of capillary vessels was counted in three randomly selected 10-power fields of view after staining with H&E and compared between the two kinds of scaffold. In animal experiment 2, two scaffolds developed from polypropylene frameworks in the omentum and two scaffolds developed from polypropylene frameworks coated with porcine atelocollagen in the omentum were analysed in the same way. The number of capillary vessels was counted in three randomly selected 10-power fields of view and compared between the two kinds of scaffold. All specimens were examined by a board-certified pathologist (T.T.).

Statistical analysis

Descriptive statistics for continuous variables are reported as mean ± standard deviation. For the comparison of continuous variables, the Mann–Whitney *U*-test was used as appropriate. All statistical tests were two-sided, and a *P*-value <0.05 was defined as statistically significant. JMP version 10.0.1 software (SAS Institute, Cary, NC, USA) was used for all analyses.

RESULTS

Clinical courses and macroscopic findings of developed composite scaffolds

All dogs uneventfully survived the sequential laparotomies in animal experiments 1 and 2.

In animal experiment 1, on reoperative laparotomies, there were minimal to mild adhesions between the abdominal wall and the omentum without peritoneal fluid. No migration was noted in frameworks placed in the omentum, whereas two (40%) polypropylene frameworks placed in the pouch of Douglas were noted to have cephalad migrations; the others involved a portion of the small bowels in the lumen (Fig. 3A, in animal experiment 1). The omentum was found to be focally hyperplastic around the framework. Regarding scaffolds developed from polypropylene frameworks in the pouch of Douglas, only thin layers (1.2 ± 0.4 mm) of connective tissue developed on the frameworks (Fig. 3B), with a minimal area of the mesh exposed, whereas homogeneously thick

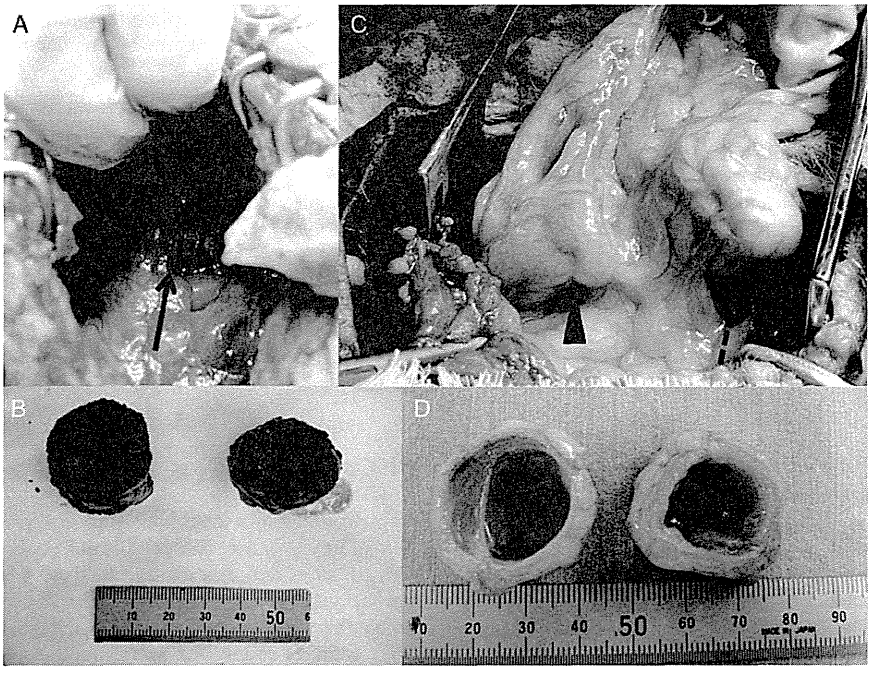

Figure 3: The developed scaffolds at reoperative laparotomies (3 weeks after placement). (**A**) The small bowels adhered to the lumen of the polypropylene framework (solid arrow) in animal experiment 1. (**B**) A scaffold developed from polypropylene framework in the pouch of Douglas (left) and in the omentum (right). (**C**) Polypropylene framework (arrowhead) and the polypropylene framework coated with porcine atelocollagen (dotted arrow) contained in the omentum in animal experiment 2. (**D**) A scaffold developed in the omentum from a polypropylene framework (left) and a polypropylene framework coated with porcine atelocollagen (right).

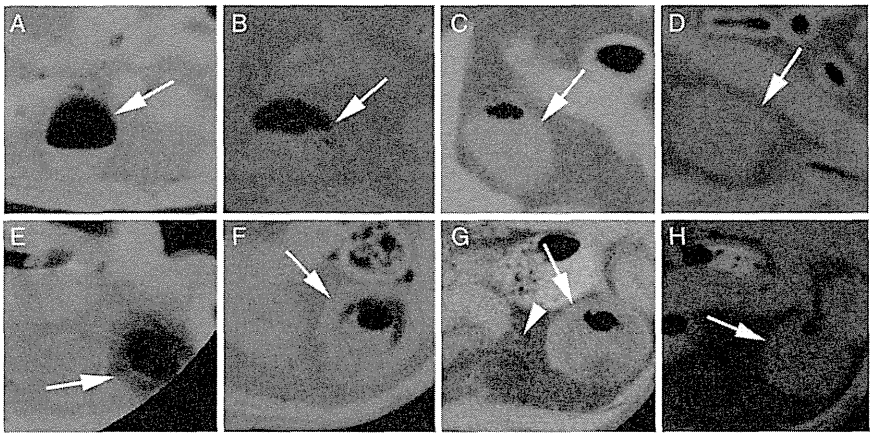

Figure 4: Abdominal computed tomography (CT) images of the polypropylene frameworks on postoperative day (POD) 0 (**A**), 7 (**B**), 14 (**C**) and 21 (**D**) and the polypropylene framework coated with porcine atelocollagen on POD 0 (**E**), 7 (**F**), 14 (**G**) and 21 (**H**) in animal experiment 2. Arrows in images show frameworks. The polypropylene framework was recognized as containing fluid that increased in volume over time (**A**–**D**). In the polypropylene framework coated with porcine atelocollagen, a layer that was shown as having mixed air and soft tissue density gradually decreased and disappeared on POD 14 (**G**), and soft tissue density growing on the framework was observed (**F**–**H**).

layers (2.6 ± 0.5 mm) developed on the frameworks in the omentum without any area exposed (Fig. 3C). Serous fluid was contained in the framework in the omentum. There was a statistically significant difference in the thickness of the connective tissue between scaffolds developed in the omentum and those in the pouch of Douglas (2.6 ± 0.5 and 1.2 ± 0.4 mm, P <0.0001).

In animal experiment 2, the omentum was found to be focally hyperplastic around the frameworks (Fig. 3C). Regarding the polypropylene frameworks or polypropylene frameworks with conjugated porcine atelocollagen from the omentum, connective tissue developed on the frameworks without any mesh exposed (Fig. 3D). Both of the developed scaffolds appeared to be waterproof and airtight and contained serous fluid. There was a statistically significant difference in the thickness of developed connective tissue between polypropylene frameworks uncoated and those with with porcine atelocollagen (2.2 ± 0.4 and 3.6 ± 0.7 mm, respectively, P <0.0001).

Radiological findings of developing composite scaffolds in the omentum on abdominal computed tomography

Representative images are shown in Fig. 4. The polypropylene framework in the omentum was recognized as containing fluid that increased in volume over time (Fig. 4A–D). The polypropylene frameworks coated with porcine atelocollagen in the omentum are shown in Fig. 4E–H, and the coating porcine atelocollagen on the framework is recognized as a layer of air mixed with soft tissue density on the lumen on POD 0 (Fig. 4E, arrow). This layer was replaced gradually with soft tissue density (Fig. 4F–H).

Histological findings of the connective tissue developed on the frameworks

In animal experiment 1, the number of capillary vessels in a 10-power field of view was 0 ± 0 in connective tissue of scaffolds developed in the pouch of Douglas and 4.5 ± 3.0 in the connective tissue of ones developed in the omentum, with a statistically significant difference ($P = 0.015$).

In animal experiment 2, the number of capillary vessels in a 10-power field of view was 3.5 ± 2.2 in the connective tissue of scaffolds developed from polypropylene frameworks in the omentum versus 5.0 ± 2.7 in the connective tissue of scaffolds developed from polypropylene frameworks coated with porcine atelocollagen in the omentum, but the difference was not statistically significant ($P = 0.15$).

The connective tissue developed on the polypropylene frameworks in the omentum in animal experiment 1 showed almost the same histological findings as that on the frameworks in the omentum in animal experiment 2. Therefore, images from animal experiment 2 are shown.

Shown in Fig. 5 are microscopic (original magnification ×10) examinations. In Fig. 5D and G, fibromuscular fibres developed and surrounded the polypropylene mesh (M) with irregular capillary vessels (arrows in magnified parts). All sections with MT staining suggested that the connective tissue was rich in collagenous fibres (Fig. 5B, E and H), produced by fibroblasts, shown with α-SMA staining (Fig. 5C, F and I).

DISCUSSION

Non-circumferential (cartilaginous portion only) replacement of a human airway with a prosthesis has already been successfully performed after resection of a cartilaginous portion of cervical trachea in 2002 [3], whereas a circumferential replacement of human airway is more challenging and was first performed by Macchiarini *et al.* in 2008 with a decellularized human tracheal graft that was cellularized by *in vitro* tissue engineering [2].

An airway prosthesis comprises a scaffold that is biological, synthetic or composite (biological and synthetic) and has tissue-engineered epithelial cells on it. It is still controversial which type

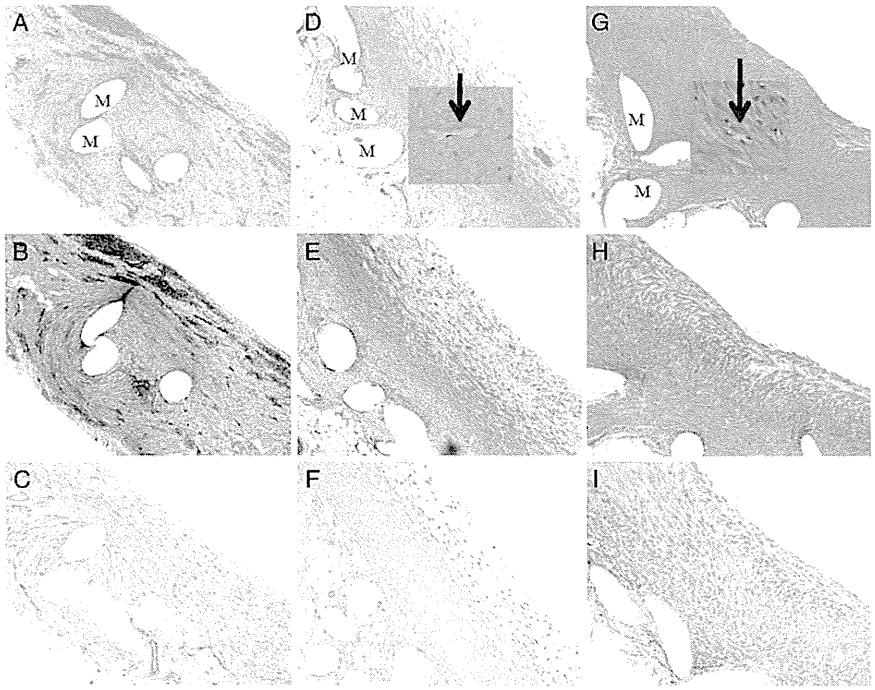

Figure 5: Sections of connective tissue of a scaffold developed from a polypropylene framework in the pouch of Douglas in animal experiment 1: (**A**) H&E staining, original magnification ×10; (**B**) MT staining, original magnification ×10; and (**C**) α-SMA staining, original magnification ×10. Sections of connective tissue of a scaffold developed from a polypropylene framework in the omentum in animal experiment 2: (**D**) H&E staining, ×10; (**E**) MT staining, ×10; and (**F**) α-SMA staining, ×10. Sections of a scaffold developed from a polypropylene framework coated with porcine atelocollagen in the omentum in animal experiment 2: (**G**) H&E staining, ×10; (**H**) MT staining, ×10; and (**I**) α-SMA staining, ×10). Fibromuscular fibres developed and surrounded the polypropylene mesh and spiral with irregular capillary vessels (indicated by an arrow in the magnified fields of **D** and **G**). In addition, lymphocytes infiltrated the connective tissue of all sections, suggesting chronic inflammatory processes. The connective tissue of all scaffolds demonstrated α-SM fibres or α-SMA (+) spindle cells with a connective tissue matrix (**C**, **F**, **I**).

of scaffold and which type of engineering are most suitable for developing an airway prosthesis. Regarding the scaffold, the advantages of a biological one included its biocompatibility and its excellent environment for cellularization by tissue engineering, whereas a synthetic scaffold has the advantages of no dependency on donors and easy handling. As for tissue engineering (prior to grafting), *in vitro* or heterotropic, it is expensive and requires technology for cell culture and implantation, whereas *in situ* tissue engineering (following grafting) has no cells on the scaffold at first and, therefore, depends on the anastomosis as a sole source for epithelial cellularization.

Airway stenosis near the anastomoses is one major problem regarding an airway prosthesis in either humans [11] or a canine model [6, 9, 10]. Macchiarini *et al.* experienced one (11.1%) with a stenosis out of nine patients in the long-term follow-up [4], while awaiting long-term (>1 year) follow-up of heterotropic tissue engineering [7]. In a canine model, the long-term incidence of anastomotic stenosis ranged from 25 to 38% without omental transposition. To resolve anastomotic stenosis and incomplete epithelialization, the omentum was previously applied in our laboratory and by other groups to wrap the anastomosis of a native airway and a prosthesis by taking advantage of its high vasculature [11–13]. The omental transposition procedure at airway grafting lowered somewhat the incidence of an anastomotic stenosis [9], but did not resolve it completely [9, 10, 12].

The omentum is known to not only vascularize other tissues, but also modulate inflammatory reactions, through which it produces connective tissue either in acute inflammatory reactions or in the subacute wound healing process [14]. Our findings in animal experiment 1 confirmed that the functions of the omentum can be applied to developing a composite scaffold for *in situ* tissue engineering, because vascularization in the scaffold is a key to successful epithelial cellularization on the scaffold [15]. Owing to its rich vasculature, the omentum appears to be superior to muscles, which are potential alternatives, in developing a composite and vascularized tracheal scaffold.

In this preliminary study, an attempt was made to develop a novel method for developing vascularized connective tissue on a synthetic framework, which could provide an excellent environment as a composite scaffold for *in situ* tissue engineering following grafting. In animal experiment 1, the control that was placed in the pouch of Douglas showed no capillary vessels in the specimen sections or an unreliable thickness (1.2 ± 0.4 mm) given that the thickness of the polypropylene mesh was 0.8 mm. In Animal experiment 2, porcine atelocollagen coating the polypropylene framework failed to show an additional benefit in vascularizing the polypropylene framework. Although the polypropylene framework coated with porcine atelocollagen in the omentum did develop thicker autologous connective tissue (3.6 ± 0.7 mm) on the scaffold, the thickness appears more than required, given that the thickness of a normal trachea is estimated to be 1–3 mm on CT [16]. Moreover, too thick connective tissue might be a barrier to neck movements. These findings suggest that porcine atelocollagen coating the polypropylene framework does not have additional benefits in developing a composite and vascularized scaffold.

The serial CT images on the polypropylene scaffold successfully identified and followed up the process of developing autologous connective tissue, which apparently plateaued between 14 and 21 days from placement. The radiological findings suggested that the development process can be tracked to some degree but revealed limitations in estimating the thickness.

The limitations of the study included use of canine models as a substitute for human subjects. In addition, the omentum can be unreliable in cases with a history of prior laparotomy and/or an upper abdominal procedure. Prior to the second stage (tracheal grafting), 3 weeks are required for connective tissue development, which is not ideal for emergent or semiemergent treatments.

Our results suggest that development of a composite tracheal scaffold with vascularized autologous connective tissue is feasible. We need to evaluate carefully the long-term outcomes of *in situ* tissue engineering in further studies, but this composite tracheal scaffold could be a reasonable alternative to our previous scaffolds or to those developed by other groups. Our next report will focus on long-term outcomes of *in situ* tissue engineering of the composite scaffolds following grafting.

Conflict of interest: none declared.

REFERENCES

[1] Jungebluth P, Bader A, Baiguera S, Möller S, Jaus M, Lim ML *et al.* The concept of in vivo airway tissue engineering. Biomaterials 2012;33:4319–26.
[2] Macchiarini P, Jungebluth P, Go T, Asnaghi MA, Rees LE, Cogan TA *et al.* Clinical transplantation of a tissue-engineered airway. Lancet 2008;372:2023–30.
[3] Omori K, Nakamura T, Kanemaru S, Asato R, Yamashita M, Tanaka S *et al.* Regenerative medicine of the trachea: the first human case. Ann Otol Rhinol Laryngol 2005;114:429–33.
[4] Jungebluth P, Moll G, Baiguera S, Macchiarini P. Tissue-engineered airway: a regenerative solution. Clin Pharmacol Ther 2012;91:81–93.
[5] Kojima K, Bonassar LJ, Roy AK, Vacanti CA, Cortiella J. Autologous tissue-engineered trachea with sheep nasal chondrocytes. J Thorac Cardiovasc Surg 2002;123:1177–84.
[6] Nakamura T, Sato T, Araki M, Ichihara S, Nakada A, Yoshitani M *et al.* In situ tissue engineering for tracheal reconstruction using luminar remodeling type of artificial trachea. J Thorac Cardiovasc Surg 2009;138:811–9.
[7] Delaere P, Vranckx J, Verleden G, De Leyn P, van Raemdonck D; Leuven Tracheal Transplant Group. Tracheal allotransplantation after withdrawal of immunosuppressive therapy. N Engl J Med 2010;362:138–45.
[8] Haag JC, Jungebluth P, Macchiarini P. Tracheal replacement for primary tracheal cancer. Curr Opin Otolaryngol Head Neck Surg 2013;21:171–7.
[9] Teramachi M, Okumura N, Nakamura T, Yamamoto Y, Kiyotani T, Takimoto Y *et al.* Intrathoracic tracheal reconstruction with a collagen-conjugated prosthesis: evaluation of the efficacy of omental wrapping. J Thorac Cardiovasc Surg 1997;113:701–11.
[10] Okumura N, Nakamura T, Natsume T, Tomihata K, Ikada Y, Shimizu Y. Experimental study on a new tracheal prosthesis made from collagen-conjugated mesh. J Thorac Cardiovasc Surg 1994;108:337–45.
[11] Gonfiotti A, Jaus MO, Barale D, Baiguera S, Comin C, Lavorini F *et al.* The first tissue-engineered airway transplantation: 5-year follow-up results. Lancet 2014;383:238–44.
[12] Nakanishi R, Shirakusa T, Mitsudomi T. Maximum length of tracheal autografts in dogs. J Thorac Cardiovasc Surg 1993;106:1081–7.
[13] Li J, Xu P, Chen H. Successful tracheal autotransplantation with two-stage approach using the greater omentum. Ann Thorac Surg 1997;64:199–202.
[14] Chandra A, Srivastava RK, Kashyap MP, Kumar R, Srivastava RN, Pant AB. The anti-inflammatory and antibacterial basis of human omental defense: selective expression of cytokines and antimicrobial peptides. PLoS One 2011;6:e20446.
[15] Nelson RJ, Goldberg L, White RA, Shors E, Hirose FM. Neovascularity of a tracheal prosthesis/tissue complex. J Thorac Cardiovasc Surg 1983;86:800–8.
[16] Webb EM, Elicker BM, Webb WR. Using CT to diagnose nonneoplastic tracheal abnormalities: appearance of the tracheal wall. Am J Roentgenol 2000;174:1315–21.

A novel surgical marking system for small peripheral lung nodules based on radio frequency identification technology: Feasibility study in a canine model

Fumitsugu Kojima, MD,[a,b] Toshihiko Sato, MD, PhD,[b] Hiromi Takahata, MEng,[c] Minoru Okada, PhD,[d] Tadao Sugiura, PhD,[d] Osamu Oshiro, PhD,[c] Hiroshi Date, MD, PhD,[b] and Tatsuo Nakamura, MD, PhD[a]

Objective: We investigated the feasibility and accuracy of a novel surgical marking system based on radiofrequency identification (RFID) technology for the localization of small peripheral lung nodules (SPLNs) in a canine model.

Methods: The system consists of 4 components: (1) micro RFID tags (13.56 MHz, 1.0 × 1.0 × 0.8 mm), (2) a tag delivery system with a bronchoscope, (3) a wand-shaped locating probe (10-mm diameter), and (4) a signal processing unit with audio interface. Before the operation, pseudolesions mimicking SPLNs were prepared in 7 dogs by injecting colored collagen. By use of a computed tomographic (CT) guide, an RFID tag was placed via a bronchoscope close to each target lesion. This was then followed by scanning with the locating probe, and wedge resection was performed when possible. Operators can locate the tag by following the sound emitted by the system, which exhibits tone changes according to the tag-probe distance. The primary outcome measure was the rate of wedge resection with good margins.

Results: A total of 10 pseudolesions imitating SPLNs were selected as targets. During thoracoscopic procedures, 9 of 10 tags were detected by the system within a median of 27 seconds. Wedge resections were performed for these 9 lesions with a median margin of 11 mm. The single failure was caused by tag dislocation to the central airway.

Conclusions: Successful localization and wedge resection of pseudolesions with appropriate margins were accomplished in an experimental setting. Our RFID marking system has future applications for accurately locating SPLNs in a clinical setting. (J Thorac Cardiovasc Surg 2014;147:1384-9)

Video clip is available online.

The accurate localization of small peripheral lung nodules (SPLNs) in a thoracoscopic setting is a challenging task, although video-assisted thoracic surgery is a more suitable approach than open surgery for small lesions.[1] In accordance with evolving patient and social demands, the importance of minimally invasive surgical procedures has increased in recent years. In 2010, the rate of video-assisted thoracic surgery reportedly reached nearly 60% of lung cancer surgery in Japan[2] and 44.7% in the United States.[3] The vast majority of SPLNs are therefore likely to be resected by a thoracoscopic approach in Japan.

Many techniques to assist the localization of SPLNs have been developed and reported; these include finger palpation, percutaneous hook-wire placement, preoperative dye marking, fluoroscopy with a contrast medium, intraoperative ultrasonography (US), and radiotracer-guided surgery.[4] These techniques have proved reliable to a certain extent, but all possess considerable problems in complications, cost, technical difficulty, and availability of facilities.[5] Consequently, there is not yet an established "best technique," and the choice of method is highly dependent on each surgeon's preference.

Despite the lack of a definitive solution for determining SPLN location, thoracic surgeons are required to manage an increasing number of small pulmonary nodules owing to the continued improvement of computed tomography (CT) technology. In 2011, the National Lung Screening Trial established the ability of low-dose CT screening to reduce mortality in a high-risk population.[6] Also, recent guidelines for lung cancer screening from The American

From the Department of Bioartificial Organs,[a] Institute for Frontier Medical Sciences, Kyoto University, Kyoto; the Department of Thoracic Surgery,[b] Kyoto University Hospital, Kyoto; the Graduate School of Engineering Science,[c] Osaka University, Toyonaka; and the Graduate School of Information Science,[d] Nara Institute of Science and Technology, Ikoma, Japan.

This project was supported by grants from The Japanese Foundation for Research and Promotion of Endoscopy, and Japan Society for the Promotion of Science Fujita Memorial Fund for Medical Research.

Disclosures: Authors have nothing to disclose with regard to commercial support.

Received for publication March 7, 2013; revisions received May 15, 2013; accepted for publication May 31, 2013; available ahead of print July 15, 2013.

Address for reprints: Toshihiko Sato, MD, PhD, Department of General Thoracic Surgery, Kyoto University, 54 Shogoin, Kyoto 6068507, Japan (E-mail: tsato@kuhp.kyoto-u.ac.jp).

0022-5223/$36.00

http://dx.doi.org/10.1016/j.jtcvs.2013.05.048

ET/BS

Abbreviations and Acronyms
CT = computed tomography
RFID = radiofrequency identification
SPLN = small peripheral lung nodule
US = ultrasonography

Association for Thoracic Surgery have recommended the surgical excision of subcentimeter lesions in patients whose tumors show suspicious changes in size or appearance.[7] For years, the preoperative marking for lung nodules smaller than 10 mm in size has also been recommended.[8] In light of these advances in CT screening and recommendations, there is an unprecedented need to improve localization techniques.

Furthermore, in this era of minimally invasive surgery, there is an increasing demand for innovative localization techniques. An ideal method not only would ensure patient safety but also would allow for adequate minimum margins from the lesion. For instance, maintenance of appropriate margins for sublobar curative resection of primary lung cancer has been shown to reduce recurrences.[9] The importance of appropriate margins has similarly been emphasized in the resection of metastatic pulmonary nodules to prevent local recurrence.[10] However, for surgeons to ensure adequate margins, they must first be able to gauge the exact distance from the target lesion to the cutting line for resection.

To address these problems, we have proposed a novel surgical marking system based on radiofrequency identification (RFID) technology, which provides a precise ranging ability.[11] In our system, 13.56-MHz micro RFID tags are used as "wireless surgical markers" to label lesions that are otherwise difficult to locate. In this study, we test the feasibility and reliability of this RFID marking system using experiments with pseudolesions imitating SPLNs in a canine model.

MATERIAL AND METHODS

RFID Marking System

The schematic diagram of our proposed RFID marking system is shown in Figure 1. The entire system consists of the following 4 main components: (1) micro RFID tags coated with polyester resin (13.56 MHz, 1.0 × 1.0 × 0.8 mm; Star Engineering Co, Ltd, Singapore), (2) tag delivery system with bronchoscope, (3) wand-shaped locating probe (10-mm diameter), and (4) signal processing unit with audio interface.

The detailed composition and algorithms of the system have been reported in our previous article.[11] The micro RFID tag works as a passive transponder without a built-in battery, with the locating probe acting as both a power supply coil and a receiver antenna. When the probe is placed in close proximity to the tag, the tag is activated by the electromagnetic field produced by the probe. The activated tag returns the response signal with a fixed wavelength of 13.56 ± 0.423 MHz. The distance between the probe and the target tag is measured by signal strength and visually presented on a monitor. The signal strength is also converted to a corresponding audio tone by the signal processing units. The operator can then accurately locate the implanted tags by scanning the target area with the probe and reacting to changes in the tone; when the probe is placed closer to the tag, the system produces a higher pitch. The prototype system used in this animal experiment had an effective range of measurement of 7 mm, and the distance can be measured down to the millimeter level.

Animal Care

Animal care, housing, and surgery were performed with the approval of the Committee for Animal Research of Kyoto University, Japan, which ensures the humane treatment of laboratory animals in compliance with guidelines established by the Ministry of Education, Culture, Sports, Science and Technology, Japan. Seven dogs (age, < 2 years; body weight, 7.5-12.5 kg) were used in this study. Before the bronchoscopic procedures, all dogs were premedicated by intramuscular injection of 0.05 mg/kg atropine sulfate. They were then sedated with intramuscular injection of 15 mg/kg ketamine hydrochloride and 3 mg/kg xylazine hydrochloride. Local anesthesia of the upper respiratory tract was performed using a 1% lidocaine solution. For surgical procedures, dogs were intubated endotracheally under the same premedication and anesthetic sedation. Sevoflurane and nitrous gas were used for maintenance of anesthesia, under mechanical ventilation. Electrocardiogram and percutaneous oxygen saturation were monitored throughout the surgical procedures.

Preparation of SPLN-Imitating Pseudolesions and Selection of Target Lesions

Before the operation, pseudolesions imitating SPLNs were created by injecting 0.2 mL of colored collagen to lung peripheral parenchyma in a selected variety of lobes under CT guidance (Aquilion TSX-101A; Toshiba, Tokyo, Japan). The colored collagen solution was prepared as a mixture of 5 mL of 1% collagen solution and 5 mL of dye (5% indocyanine green or indigocarmine). A 23-gauge injection needle (NM-201L-0423; Olympus Corporation, Tokyo, Japan) was used for injecting the solution through the working channel of the bronchoscope (BF240; Olympus). A postprocedure CT scan was performed to confirm the size and location of each created lesion. Peripherally located pseudolesions with a diameter of approximately 10 mm were selected as target lesions for further experimentation.

Marking of the Target Lesions

The target lesions were marked within 2 days after creation for the subsequent operative procedures. Under a CT scan guide, an RFID tag was delivered into a small peripheral airway close to each target lesion. Through the 2-mm working channel of the bronchoscope, an introducer tube with a radiopaque marker on its distal tip was navigated to the target lesion (Figure 2). The tube was constructed from polytetrafluoroethylene (Teflon; DuPont Corporation, Wilmington, Del) and has an outer diameter of 1.8 mm. When the operator confirmed that the tip of the introducer tube was in the vicinity of the target lesion, the tag could then be implanted: the RFID tag was inserted from the proximal end of the tube and pushed out from the distal end by a flexible pusher-wire made of stainless steel. A postprocedure CT scan was performed to measure the distance from the tag to the nearest edge of the target lesion.

Operative Procedure

Immediately after tag delivery to the target lesions, the dogs were brought into an operating room and placed in a lateral decubitus position. With the animals under general anesthesia with intubation and ipsilateral lung collapse, the embedded tag and wedge resection of the target lesion were detected. Three ports with a 10-mm incision were set for each tag—1 for the scope and 2 for port access to the pleural cavity. Under thoracoscopic view, the lobe of interest was scanned with the locating probe to find the target lesion labeled with the tag. When the tag was localized, ring-shaped forceps were introduced from the other port to grasp the pleura just

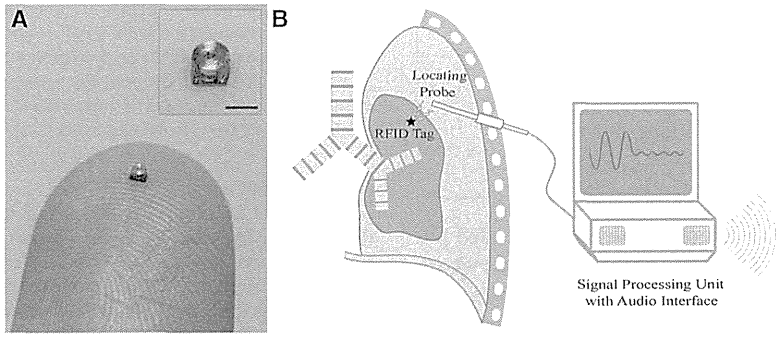

FIGURE 1. A, Photograph of a micro radiofrequency identification *(RFID)* tag on a forefinger (scale bar = 1 mm). The tag works as a passive transponder when it is activated by a radio wave of 13.56 MHz. B, Schematic diagram of the RFID marking system, including a wand-shaped locating probe for endoscopic use and a signal processing unit with an audio interface. The operator can locate the implanted tags by scanning the target area with the probe and responding to audio cues; when the probe is nearer the tag, the system produces a higher pitch.

above the site. After a reconfirmation of the tag position, the locating probe was pulled off and an endostapler was introduced from the same port to clamp the estimated resection line. Before the endostapler was fired, the locating probe was reinserted in place of the ring forceps to establish that the tag was contained within the lung tissue to be excised (Figure 3). Owing to the millimeter-level ranging capability of the system, an appropriate surgical margin could be ensured. When the lesion and the tag were resected with the endostaplers, the specimen was incised to measure the surgical margin.

Outcome Measures

The primary end point of this study was the rate of successful wedge resection of pseudolesions with good margins. Secondary measures were (1) the distance from the pseudolesion to the tag as shown in the confirmation CT, (2) the time required for the marking procedure, (3) the time required for tag detection at operation, and (4) the distance from the edge of the pseudolesion to the stapler line, which provides information on the surgical margins (Table 1). The median values and range were calculated for these measures. Finally, we analyzed the system's merits and pitfalls.

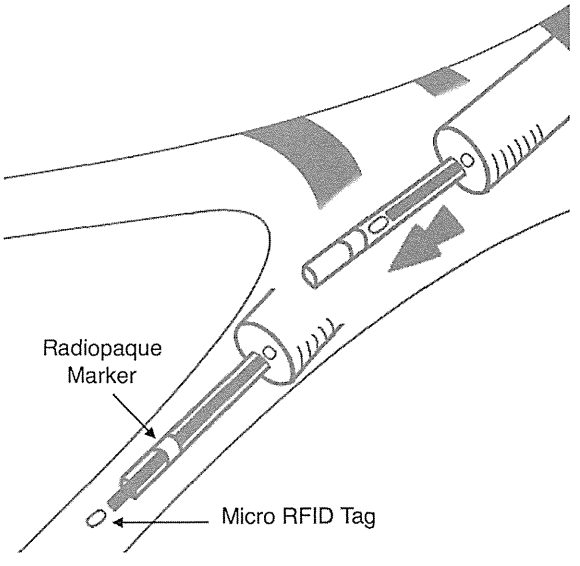

FIGURE 2. Illustration of the radiofrequency identification *(RFID)* tag delivery system. An introducer tube with a radiopaque marker on its distal tip is inserted through the 2-mm channel of a bronchoscope. The material of the tube is polytetrafluoroethylene (Teflon). An RFID tag is inserted from the proximal end of the tube and pushed out from the distal end by a pusher-wire.

RESULTS

A total of 14 pseudolesions were created by colored collagen injection in 7 dogs. Of the 14 pseudolesions, 10 had a diameter of approximately 10 mm and were selected as target lesions for further experimentation; there were 2 pseudolesions located in the right cranial lobes, 4 in the right caudal lobes, and 4 in the left caudal lobes. The other 4 pseudolesions were excluded because of larger diffusion or intrabronchial spread of injected collagen solution.

By means of the bronchoscopic marking procedures, each selected pseudolesion was accurately labeled with 1

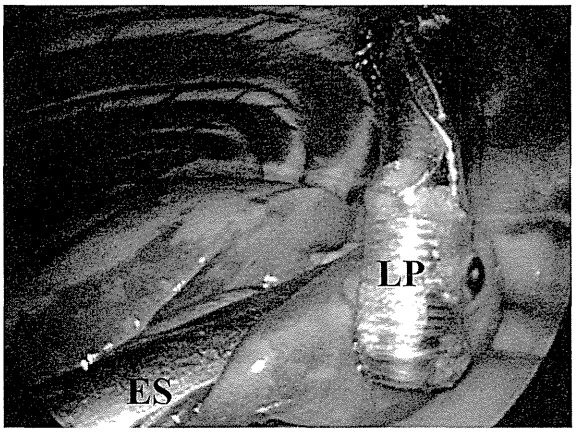

FIGURE 3. Thoracoscopic view of tag detection with a locating probe *(LP)* and resection of a pseudolesion in peripheral lung parenchyma. Before firing off the endostapler *(ES)*, the operator can confirm the position of the implanted tag to ensure an appropriate margin.

ET/BS

TABLE 1. Results of the primary end point and secondary outcome measures of the experiments

Primary end point		
Successful tag detection*	9/10	
Successful wedge resection*	9/10	
Secondary measures		**Median**
Time required for marking (min)	5-34	11
Distance from the lesion to the tag (mm)	0-6.5	2.1
Time required for tag detection (s)†	10-105	27
Surgical margin (mm)†	8-12	11

*One failure was due to dislocation of the tag. †n = 9.

RFID tag (Figure 4). The tags were placed at a median distance of 2.1 mm from the lesions (range, 0-6.5 mm, confirmed by postprocedure CT scan). The time required for the marking procedure ranged from 5 to 34 minutes (median, 11 minutes) from the insertion of the bronchoscope to the completion of the confirmation CT scan. Marking procedures were performed just after the creation and selection of the first 3 target pseudolesions and 1 or 2 days after creation for the other 7. No major complications such as pneumothorax or bleeding were observed.

During the thoracoscopic surgical procedures, 9 of the 10 implanted tags were successfully detected by the system. The time required for detection ranged from 10 to 105 seconds (median, 27 seconds). Subsequently, wedge resections were performed for these 9 lesions with a median margin of 11 mm (range, 8-12 mm). In the single nondetected case, a right upper lobectomy was performed only to find no tag in the resected lobe. The dislocated tag was later found in the endotracheal tube.

DISCUSSION

RFID is a wireless method of automatic identification originally developed for military radar systems in the 1940s to distinguish between friendly and enemy aircraft.[12] Currently, RFID tags are indispensable in modern society, with applications in item tracking for supply chain management, cashless payments for shopping, and personal identification for ticketing or entrance gates. The continuing miniaturization of RFID tags and development of computer networks have contributed to the widespread use of this system.

Applications have also developed in the field of health care: RFID technology has become widely used for personal identification of medical staff and for tracking drugs and medical equipment in so-called "smart hospitals."[13] Some reports have been published in which RFID technology was deployed to solve problems specific to medical practice. For example, Macario and colleagues[14] successfully detected surgical sponges labeled with RFID tags in the abdomen, Reicher and colleagues[15] reported the efficacious monitoring of the position of an RFID tag–labeled endotracheal tube at bedside, and Mayse and colleagues[16] experimentally implanted RFID tags in canine airways to achieve real-time tracking of tumor positions for stereotactic radiotherapy. In all these medical cases, RFID technology was used to detect the position of an embedded tag.

Our idea was to use micro RFID tags as wireless markers for locating SPLNs in thoracoscopic lung surgery. There is currently only a single previous report showing a similar concept in the field of breast surgery.[17] That study was essentially a proof of concept in a phantom study using large-sized tags (2 mm in diameter and 8 or 12 mm in length) responding to a radiofrequency of 134.2 kHz. To our knowledge, there has been no report on animal experiments or clinical trials of the system, although their tags (VeriChip; Verimed, Inc, Fort Lauderdale, Fla) have been approved by the United States Food and Drug Administration for human use. With the further advances in RFID technology, we have used 1-mm RFID tags in this study and confirmed their feasibility in an animal model for lung wedge resection.

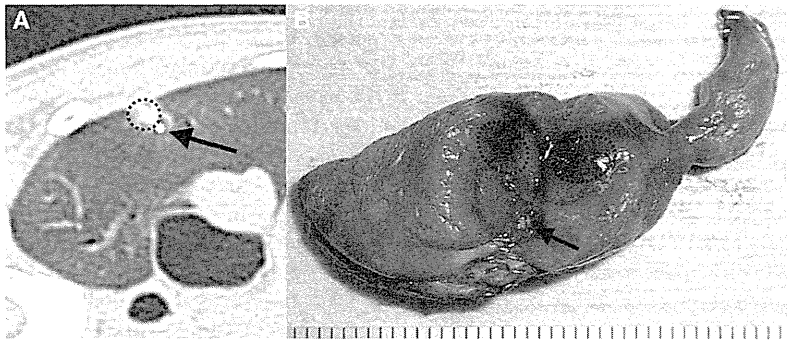

FIGURE 4. A, Computed tomography scan of a canine lung, including a pseudolesion created by colored collagen injection (areas surrounded by *black dotted line*) and an implanted micro radiofrequency identification tag *(black arrow)*. B, Photograph of a corresponding surgical specimen (scale bar = 1 mm).

ET/BS

Locating an SPLN has been a challenging task since the era of open thoracotomies. It is even more difficult in a thoracoscopic situation because finger palpation is far less effective. As a consequence, many techniques to assist in the localization of SPLNs have been innovated, with these techniques broadly belonging to 1 of 2 completely different strategies: intraoperative techniques (eg, finger palpation and ultrasound) and preoperative placement of a marker (eg, hook-wire, dye, contrast medium, and radiotracer).[4]

Intraoperative techniques have the virtue of noninvasiveness, and to our knowledge no major complications as a result of these techniques have been reported. Even though intraoperative US is more effective than finger palpation, with a success rate of 70% to 100 % in selected patients,[4] this technique has several limitations.[5] Successful localization using intraoperative US is highly dependent on operator skill. Also, localization is difficult in cases of emphysematous change or incomplete collapse of the target lung. Success rates are further reduced in cases of small nodules less than 1 cm in size or deep lesions more than 1 cm from the visceral pleura. Soft nodular ground-glass opacities observed in bronchoalveolar cell carcinomas are also difficult to localize using US. Because of these limitations, intraoperative US has little versatility as a localization technique.

The use of markers is a viable option for surgeons to overcome the limitations of intraoperative localization techniques. The implantation or delivery procedures of several kinds of markers can be classified into 2 categories according to their approaches: a percutaneous pneumocentesis approach and a transbronchial approach with a bronchoscope. Generally, percutaneous implantation of a marker is highly associated with complications such as pneumothorax (8%–50%), pulmonary hemorrhage (12%–35%), and pleuritic pain (5%–6%).[4] In addition, several authors have raised caution on the risk of fatal air embolisms induced by hook-wire implantation.[18] In contrast, the transbronchial approach can theoretically eliminate the risk of complications related to the percutaneous approach. In our experiments, no major complications were observed related to bronchoscopic delivery of RFID tags, and the time required for marking ranged from 5 to 34 minutes (median, 11 minutes). Bronchoscopic procedures can be a distressing experience for patients, but the transbronchial approach is less invasive than the percutaneous approach.

However, some markers have been used despite their negative aspects. Time constraints are the main cause of failure in the case of dye or radiotracer marking, as the diffusion of dyes and the decay of radiotracers prevent surgeons from successful localization of SPLNs. These shortcomings also lead to difficulties in scheduling preoperative procedures and surgical resection. It has been recommended that surgery be performed within 24 hours after injection of dye and within 12 hours after radiotracer administration.[4,5] The RFID marking system is free from these time constraints and can provide flexibility in the time interval between the marking procedure and surgery.

In the context of intraoperative fluoroscopy, a contrast medium (ie, barium or lipiodol) is consistently reported as the most effective and reliable marker: Watanabe and colleagues[19] reported a success rate of 100% from their experience of 174 nodules; Asano and associates[20] emphasized a success rate of 100% for 31 pure ground-glass nodules less than 10 mm in size; and Okumura and coworkers[21] stated that good surgical margins could be assured with this technique and that multiple markings can be achieved by transbronchial injection of barium with minimum invasiveness. Unfortunately, despite these merits, the radiation exposure for operators and patients cannot be overlooked. Unnecessary exposure to medical radiation should be avoided if possible, and the use of RFID technology presents an alternative for the purpose of SPLN localization.

The RFID marking system has several positive aspects. The first merit is that of quick detection with simple operability. The system requires only a locating probe in the surgical field. During thoracoscopic surgical procedures, localization of the RFID tag was promptly achieved without the need for unwieldy instruments such as a fluoroscope. As shown in our experiments, the time required for tag detection after insertion of the locating probe ranged from 10 to 105 seconds (median, 27 seconds). Quick detection of the tag and swift localization of the target lesion were achieved by simply listening and reacting to the audio cues from the system; there was no need for operators to shift their gaze from the surgical field or the monitor for the thoracoscope. The simple operability of the system also exempts thoracic surgeons from having to become skilled in an unfamiliar technique such as US interpretation or from the threat of radiation exposure. The second and more important merit is that the 1-mm small wireless marker enables the pinpoint localization of target lesions; the system provides millimeter-level ranging capability to enhance localization accuracy. As a consequence, an appropriate distance from the lesion to the resection line is ensured because the operator can confirm that the RFID marker is included within the lung parenchyma to be resected. In our study with pseudolesions, surgical margins of resected specimens ranged from 8 to 12 mm (median, 11 mm). Accurate localization enables thoracic surgeons to perform sublobar resections with reduced risk of local recurrence in a short procedure time. Third, the labeling of multiple lesions or multiple marking of a single lesion can be achieved in this system because each tag has its own unique identifiable number.

This study has the following limitations. Our prototype system has an effective communication range of 7 mm, mainly owing to limitations in the power supply from the locating probe. Although 7 mm is adequate for animal experiments, an effective range of 30 mm may be required

for clinical use in human lungs. Improvements to the effective range are in progress and can be achieved with further customization of the tag and the probe.

The second limitation is that dislocation of the implanted tag is a problem of critical importance for the RFID marking system. The reason for the sole detection failure in our experiments was the dislocation of the tag to the central airway. To address this problem, we are developing a tag anchoring function. For the purpose of lung tumor tracking during radiation therapy, the use of an RFID tag with anchoring legs was reported to have an 87% successful stabilization rate for a period of 60 days.[22] In addition to the anchoring function, the coating of RFID tags is another modification under consideration owing to the possibility of accidental ingestion of a dislocated tag into the digestive tract.

The third limitation is related to the safety of the system. We did not encounter any instances of adverse effects caused by the tag, but the study period was limited to 3 days at its longest. The safety of the in vivo use of RFID tags has been endorsed by long-term experiments in a canine subcutaneous implantation model,[23] as well as by routine use in livestock farming. Although we have had limited experience with RFID tag placement into a small airway, Mayse and coworkers[16] have reported no complications in similar experimental implantation of 60 days. To our knowledge, no other published report has described the long-term implantation effects of RFID tags into airways. Further investigation is therefore required into the safety of this system.

The additional cost, time, and radiation exposure could be a demerit of this new method. However, the preoperative marking procedure under CT guidance may be appropriate for cases in which the target is a small peripheral lesion that is difficult to locate under fluoroscopy. RFID tags in commercial mass production are expected to be similar in cost to conventional markers including hook-wires or dye. In general, we estimate that the additional cost, time, and radiation exposure for the RFID marking method are expected to be in the same range as conventional methods that require CT guidance. A cost-benefit analysis is required to determine the best role and use of such techniques in the management of small peripheral lung nodules.

CONCLUSIONS

The feasibility of our RFID marking system for SPLN localization was demonstrated in a canine model. Further developmental work is underway to improve the effective range, to equip the tags with an anchoring function, and to confirm the safety in implantation.

We are indebted to Mr Tominaga Yukio (Star Engineering Co Ltd, Hitachi, Japan) for his technical help in preparing micro RFID tag. We also thank Miss Mani Sato for preparing nice illustrations.

References

1. Landreneau RJ, Mack MJ, Dowling RD, Luketich JD, Keenan RJ, Ferson PF, et al. The role of thoracoscopy in lung cancer management. *Chest*. 1998;113: 6S-12S.
2. Kuwano H, Amano J, Yokomise H. Thoracic and cardiovascular surgery in Japan during 2010: annual report by The Japanese Association for Thoracic Surgery. *Gen Thorac Cardiovasc Surg*. 2012;60:680-708.
3. Boffa DJ, Kosinski AS, Paul S, Mitchell JD, Onaitis M. Lymph node evaluation by open or video-assisted approaches in 11,500 anatomic lung cancer resections. *Ann Thorac Surg*. 2012;94:347-53; discussion 353.
4. Sortini D, Feo C, Maravegias K, Carcoforo P, Pozza E, Liboni A, et al. Intrathoracoscopic localization techniques. Review of literature. *Surg Endosc*. 2006;20: 1341-7.
5. Daniel TM. A proposed diagnostic approach to the patient with the subcentimeter pulmonary nodule: techniques that facilitate video-assisted thoracic surgery excision. *Semin Thorac Cardiovasc Surg*. 2005;17:115-22.
6. Aberle DR, Adams AM, Berg CD, Black WC, Clapp JD, Fagerstrom RM, et al. Reduced lung-cancer mortality with low-dose computed tomographic screening. *N Engl J Med*. 2011;365:395-409.
7. Jaklitsch MT, Jacobson FL, Austin JH, Field JK, Jett JR, Keshavjee S, et al. The American Association for Thoracic Surgery guidelines for lung cancer screening using low-dose computed tomography scans for lung cancer survivors and other high-risk groups. *J Thorac Cardiovasc Surg*. 2012;144:33-8.
8. Suzuki K, Nagai K, Yoshida J, Ohmatsu H, Takahashi K, Nishimura M, et al. Video-assisted thoracoscopic surgery for small indeterminate pulmonary nodules: indications for preoperative marking. *Chest*. 1999;115:563-8.
9. Schuchert MJ, Abbas G, Awais O, Pennathur A, Nason KS, Wilson DO, et al. Anatomic segmentectomy for the solitary pulmonary nodule and early-stage lung cancer. *Ann Thorac Surg*. 2012;93:1780-5.
10. Welter S, Theegarten D, Trarbach T, Maletzki F, Stamatis G, Tötsch M. Safety distance in the resection of colorectal lung metastases: a prospective evaluation of satellite tumor cells with immunohistochemistry. *J Thorac Cardiovasc Surg*. 2011;141:1218-22.
11. Takahata H, Kojima F, Okada M, Sugiura T, Sato T, Oshiro O. Thoracoscopic surgery support system using passive RFID marker. In: Engineering in Medicine and Biology Society (EMBC). 2012 Annual International Conference of the IEEE. 2012:183-186.
12. Stockman H. Communication by means of reflected power. *Proc IRE*. 1948;36: 1196-204.
13. Fuhrer P, Guinard D. Building a Smart HospitNonEning RFID technologies. European Conference on eHealth. 2006;5.
14. Macario A, Morris D, Morris S. Initial clinical evaluation of a handheld device for detecting retained surgical gauze sponges using radiofrequency identification technology. *Arch Surg*. 2006;141:659-62.
15. Reicher J, Reicher D, Reicher M. Use of radio frequency identification (RFID) tags in bedside monitoring of endotracheal tube position. *J Clin Monit Comput*. 2007;21:155-8.
16. Mayse ML, Parikh PJ, Lechleiter KM, Dimmer S, Park M, Chaudhari A, et al. Bronchoscopic implantation of a novel wireless electromagnetic transponder in the canine lung: a feasibility study. *Int J Radiat Oncol Biol Phys*. 2008;72:93-8.
17. Reicher JJ, Reicher MA, Thomas M, Petcavich R. Radiofrequency identification tags for preoperative tumor localization: proof of concept. *AJR Am J Roentgenol*. 2008;191:1359-65.
18. Sakiyama S, Kondo K, Matsuoka H, Yoshida M, Miyoshi T, Yoshida S, et al. Fatal air embolism during computed tomography–guided pulmonary marking with a hook-type marker. *J Thorac Cardiovasc Surg*. 2003;126:1207-9.
19. Watanabe K, Nomori H, Ohtsuka T, Kaji M, Naruke T, Suemasu K. Usefulness and complications of computed tomography–guided lipiodol marking for fluoroscopy-assisted thoracoscopic resection of small pulmonary nodules: experience with 174 nodules. *J Thorac Cardiovasc Surg*. 2006;132:320-4.
20. Asano F, Shindoh J, Shigemitsu K, Miya K, Abe T, Horiba M, et al. Ultrathin bronchoscopic barium marking with virtual bronchoscopic navigation for fluoroscopy-assisted thoracoscopic surgery. *Chest*. 2004;126:1687-93.
21. Okumura T, Kondo H, Suzuki K, Asamura H, Kobayashi T, Kaneko M, et al. Fluoroscopy-assisted thoracoscopic surgery after computed tomography–guided bronchoscopic barium marking. *Ann Thorac Surg*. 2001;71:439-42.
22. Shah AP, Kupelian PA, Willoughby TR, Meeks SL. Expanding the use of real-time electromagnetic tracking in radiation oncology. *J Appl Clin Med Phys*. 2011;12:3590.
23. Murasugi E, Koie H, Okano M, Watanabe T, Asano R. Histological reactions to microchip implants in dogs. *Vet Rec*. 2003;153:328-30.

ET/BS

The Laryngoscope

Restoration of Scarred Vocal Folds Using 5 Amino Acid-Deleted Type Hepatocyte Growth Factor

Masanobu Mizuta, MD; Shigeru Hirano, MD, PhD; Satoshi Ohno, MD, PhD; Shin-ichi Kanemaru, MD, PhD; Tatsuo Nakamura, MD, PhD; Juichi Ito, MD, PhD

Objectives/Hypothesis: Our previous studies demonstrated a regenerative effect of recombinant human hepatocyte growth factor (HGF) on vocal fold scarring using full-length HGF. However, clinical application has not yet been achieved because of the lack of a good manufacturing practice (GMP) for full-length HGF. Another natural form of human HGF, 5 amino acid-deleted type HGF (dHGF), has been newly produced under a GMP procedure. In the current study, we investigated the effect of dHGF in comparison with full-length HGF for the treatment of vocal fold scars using a canine model.

Study Design: Prospective animal experiment.

Methods: The vocal folds of nine beagles were unilaterally injured. Four weeks after injury, the vocal folds were treated with an intracordal injection of full-length HGF (full HGF group), dHGF (dHGF group), or phosphate-buffered saline (sham group). Vibratory and histological examinations were performed for each group 6 months after injury.

Results: Vibratory examinations demonstrated significantly lower phonation threshold pressure and a higher ratio of normalized mucosal wave amplitude in both the full HGF and dHGF groups as compared to the sham group. Histological examination showed restoration of hyaluronic acid in both the full HGF and dHGF groups as compared to the sham group. No significant differences were observed for each parameter between the full HGF group and the dHGF group.

Conclusions: dHGF showed the same potential for regenerative effects on vocal fold scars as full-length HGF. dHGF should be applicable for human clinical trials in patients with vocal fold scars.

Key Words: Vocal fold scarring, 5 amino acid-deleted type hepatocyte growth factor.

Level of Evidence: NA

***Laryngoscope*, 124:E81–E86, 2014**

INTRODUCTION

The vocal fold has an ideal viscoelasticity that enables rapid mucosal vibration to produce sounds. Vocal fold scars develop as a consequence of injury and inflammation of the mucosa, which causes the folds to stiffen and difficulties in vibration.[1] Once the vocal fold is scarred, severe dysphonia or aphonia occurs. Previous histological studies using animals and humans revealed increased deposition of disorganized collagen, a reduction of hyaluronic acid, elastin, decorin, and fibromodulin, and an increase of fibronectin.[2–6] Thick collagen deposition and loss of hyaluronic acid (HA) are regarded as particularly detrimental and need to be addressed in the treatment of vocal fold scars.

Hepatocyte growth factor (HGF) was originally identified and cloned as a potent mitogen for mature hepatocytes.[7,8] It is multipotent and is able to regenerate several organs and tissues due to its strong angiogenic, antifibrotic, and antiapoptosis activities.[7,8] Human HGF has two natural forms: one is full-length HGF composed of 697 amino acid residues and the other is a 5 amino acid-deleted type HGF (dHGF), which lacks the F-L-P-S-S amino acid residues in the first kringle domain.[7,9,10] We have demonstrated that full-length HGF stimulates protein production and gene expression of extracellular matrix molecules in the vocal fold mucosa.[11–16] Specifically, full-length HGF stimulates HA and matrix metalloproteinase-1 synthesis by fibroblasts in the vocal folds. This function is regarded as having a therapeutic potential for treatment of vocal fold scars. In addition, our previous animal experiments demonstrated that locally applied full-length HGF improves the vibratory properties of scarred vocal folds. There was restoration of histology including digestion of collagen and deposition of HA.[17,18] We also confirmed that delivery of full-length HGF with a gelatin hydrogel strengthened the regenerative effects, even for chronic scars of the vocal fold.[19, 20] Together, these findings demonstrate the

From the Department of Otolaryngology–Head and Neck Surgery (M.M., S.H., S.-I.K., J.I.), Graduate School of Medicine, Kyoto University, Kyoto, Japan; Department of Otolaryngology (S.O.), Wakayama Red Cross Hospital, Wakayama, Japan; Department of Regenerative Treatment for Tympanic Membrane (S.-I.K.), The Foundation for Biomedical Research and Innovation, Kobe, Japan; Department of Otolaryngology (S.-I.K.), Kitano Hospital, Tazuke Kofukai Medical Research Institute, Osaka, Japan; Department of Bioartificial Organs (T.N.), Institute for Frontier Medical Sciences, Kyoto University, Kyoto, Japan

Editor's Note: This Manuscript was accepted for publication August 26, 2013.

This study was supported by the Advanced Research for Medical Products Mining Program of the National Institute of Biomedical Innovation (NIBIO).

The authors have no other funding, financial relationships, or conflicts of interest to disclose.

Send correspondence to Shigeru Hirano, MD, Department of Otolaryngology–Head and Neck Surgery, Graduate School of Medicine, Kyoto University, Sakyo-ku, Kyoto 606-8507, Japan.
E-mail: hirano@ent.kuhp.kyoto-u.ac.jp

DOI: 10.1002/lary.24413

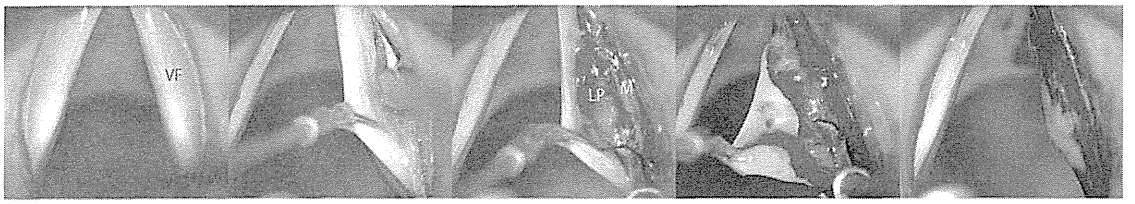

Fig. 1. Surgical procedure. The vocal folds were unilaterally scarred by stripping the entire layer of the lamina propria down to the muscle under a direct laryngoscope. LP = lamina propria; M = muscle; VF = vocal fold. [Color figure can be viewed in the online issue, which is available at wileyonlinelibrary.com.]

regenerative effects of full-length HGF on vocal fold scars. However, clinical application has not yet been achieved because of a lack of a good manufacturing practice (GMP) for full-length HGF.

Recently, recombinant human dHGF has been produced by a GMP procedure. It was confirmed that dHGF has the same biological activities as full-length HGF, and it was slightly more potent under specific conditions.[10] However, it is unclear whether dHGF has the same effects on vocal fold scars as full-length HGF. In the current study, we examined the regenerative effects of dHGF on scarred vocal folds using a canine model and compared it with full-length HGF.

MATERIALS AND METHODS

Animals

Nine beagles weighing 8 to 13 kg were used in this study. All experimental protocols were approved by the Animal Committee of the Graduate School of Medicine, Kyoto University. Animal care was provided under the supervision of the Institute of Laboratory Animals of the Graduate School of Medicine, Kyoto University.

Preparation of HGF Injection

Full-length recombinant human HGF (full HGF) was purchased from Sigma-Aldrich Co. (St. Louis, MO). dHGF was supplied by Kringle Pharma, Inc. (Osaka, Japan). Both full HGF and dHGF were diluted with phosphate-buffered saline containing 0.5 % human serum albumin to avoid adsorption loss.

Surgical Procedure

The surgical procedures that were used for generating vocal fold injuries have been established in previous studies.[17,19,20] All animals were sedated under general anesthesia with an intramuscular injection of ketamine hydrochloride (15 mg/kg) and xylazine hydrochloride (6 mg/kg). The glottis was visualized using a direct laryngoscope and the vocal folds were unilaterally scarred by stripping the entire layer of the lamina propria down to the muscle with microscissors and microforceps (Fig. 1). The contralateral vocal folds were kept intact as normal controls. The sides for scarring were randomly selected.

Injection Procedure

At 4 weeks after the initial injury, the scarred vocal folds were treated with a transcordal injection of one of three different materials: 1) full HGF (full HGF group, 0.5 mL, 1 μg/mL), 2) dHGF (dHGF group, 0.5 mL, 1 μg/mL), or 3) phosphate-buffered saline (sham group, 0.5 mL). The same injection was repeated twice with an interval of 1 week between injections for each group.

Experimental animals were euthanized 6 months after the initial injury. They were sedated as described above and euthanized with an intracardiac injection of pentobarbital sodium (25 mg/kg). Larynges were harvested immediately and used for vibratory examinations and were subsequently subjected to histological examination.

Vibratory Examination of Excised Larynges

Vocal fold vibrations were examined using an excised larynx setup described in previous studies.[20] For better visualization of the vocal fold, supraglottic structures such as the epiglottis, false vocal folds, and aryepiglottic folds were removed after resection of the superior portion of the thyroid cartilage. The arytenoid cartilages were sutured together, and an arytenoid adduction procedure was performed bilaterally using 3-0 Prolene to close the glottis. Once the larynx was mounted, an endotracheal tube was inserted and clamped to prevent air leaks. Air was pumped through the tube to generate vocal fold vibrations. Larynges were irrigated with saline throughout the experiment to keep the vocal folds moist. A high-speed digital imaging system (Memrecam Ci; NAC Image Technology, Osaka, Japan) was used to record vocal fold vibrations from the superior view. The camera was mounted 50 cm above the larynx, and the image was displayed on a monitor. The images were recorded at a frame rate of 2,000 to 4,000 frames per second, and the images were then scanned into a computer (Fig. 2).

Phonation threshold pressure (PTP) was used as one of the functional parameters of the mucosal vibration. PTP, which is regulated by factors such as vocal fold thickness, property, and glottal width, was defined as the minimum amount of subglottal pressure required to initiate vocal fold oscillation. Further, the amplitude of the mucosal wave was measured to evaluate the mucosal vibration and elasticity of the vocal fold structures, namely the lamina propria, using ImageJ software (National Institutes of Health, Bethesda, MD) (Fig. 3). The distance (d1) from the midline of the glottis to the edge of the vocal fold was measured at the anteroposterior middle portion of the vocal fold during the closed phase. The closed phase was determined based on the motion of the upper and lower lips of the vocal folds. The same distance (d2) was measured at the maximum open phase. The mucosal wave amplitude was defined by subtracting d1 from d2 and was normalized by dividing the subtracted digit by the anteroposterior length of the glottis (L), which was measured from the anterior commissure to the vocal process. The following formula was used: normalized mucosal wave amplitude (NMWA) = (d2 − d1)/L.

To compare the NMWA of the treated side with the normal side, we calculated the ratio of the NMWA. The following formula was used: the ratio of NMWA = (NMWA of the treated vocal fold)/(NMWA of the control vocal fold, contralateral side).

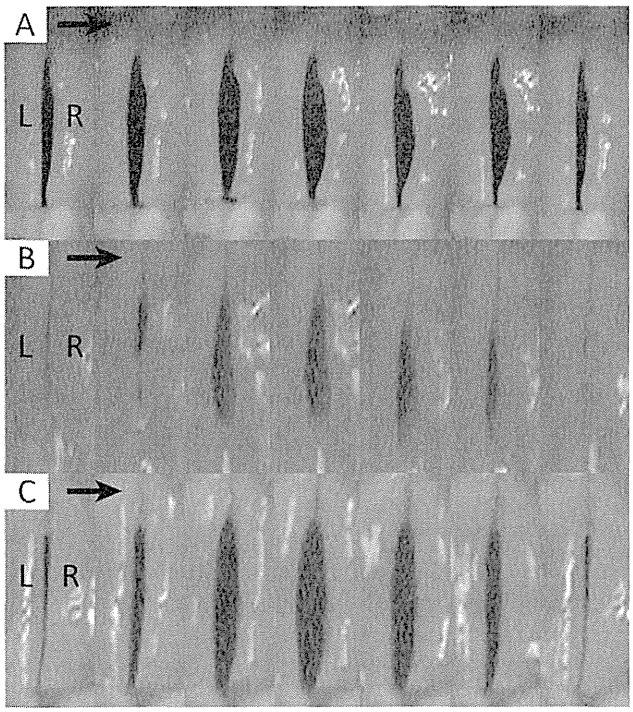

Fig. 2. Digital high-speed images of vocal fold vibratory patterns during vibratory examination of the excised larynx. (A) Sham group. (B) Full-length hepatocyte growth factor (full HGF) group. (C) 5 amino acid-deleted type HGF (dHGF) group. The full HGF-treated vocal folds and dHGF-treated vocal folds showed better mucosal vibration and a smaller glottal gap during the closed phase than the sham-treated vocal folds. L = normal side; R = treated side.

Normalized glottal gap (NGG) was calculated to evaluate glottis closure during the closed phase. The glottal gap area (a) was measured using ImageJ software and was normalized by dividing it by L^2. The following formula was used: $NGG = a/L^2 \times 100$.

Histological Examination

After vibratory examination, the larynges were fixed in 10% formaldehyde for tissue examination. Larynges were subsequently embedded in paraffin, and 5-μm-thick serial sections were prepared in the coronal plane from the anteroposterior middle portion of the vocal folds. Elastica van Gieson staining was performed to identify collagen and elastin. Alcian blue staining was performed on serial sections with or without hyaluronidase digestion to identify HA. Images were captured with a Biorevo BZ-9000 microscope (Keyence Corp., Osaka, Japan). The sections were examined at 4× to 40× magnification. On Alcian blue-stained sections, the blue-stained areas of the lamina propria were measured using software that automatically measures an area with a designated color threshold (Biorevo BZ-H1C and BZ-H1M; Keyence Corp.). The color threshold was designated by the examiner. The ratio of the stained area to the total area of the lamina propria was then calculated for each section. The amount of HA in the lamina propria was determined by subtracting the ratio of the blue-stained area of the section with hyaluronidase digestion from that of an adjacent section without digestion.[21] These assessments were performed in a blinded fashion, in which the examiners were not informed of the group to which each slide belonged.

Statistical Analysis

Statistical analyses were performed using one-way factorial analysis of variance (ANOVA) followed by a post hoc Scheffé test. Statistical significance was defined as $P < .05$.

RESULTS

Vibratory Examination of Excised Larynges

In digital high-speed images of vocal fold vibratory patterns during vibratory examination, the injured vocal folds in the full HGF group and the dHGF group showed better vibration than the sham-treated vocal folds, which had limited vibratory movement (Fig. 2). The vocal folds of the full HGF and dHGF groups resembled the normal vocal folds on the contralateral side.

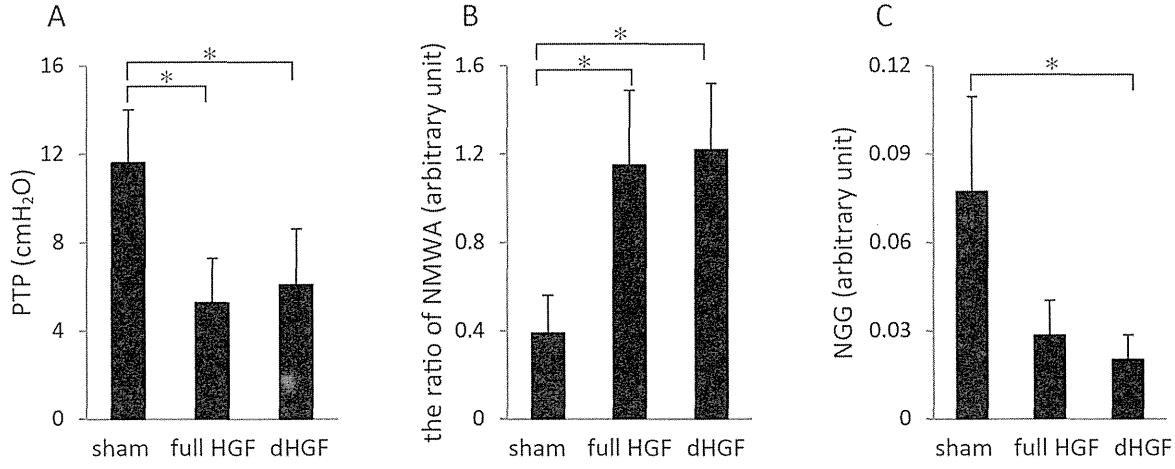

Fig. 3. Results of the vibratory examinations. The full hepatocyte growth factor (HGF) group and the 5 amino acid-deleted type HGF (dHGF) group showed significantly lower phonation threshold pressure (PTP) (A) and a higher ratio of normalized mucosal wave amplitude (NMWA) (B) than the sham group. The dHGF group showed a smaller normalized glottal gap (NGG) (C) than the sham group. No significant differences were observed for each parameter between the full HGF group and the dHGF-treated group. *Significant difference ($P < .05$) compared to the sham-treated group (one-way factorial analysis of variance, post hoc Scheffé test).

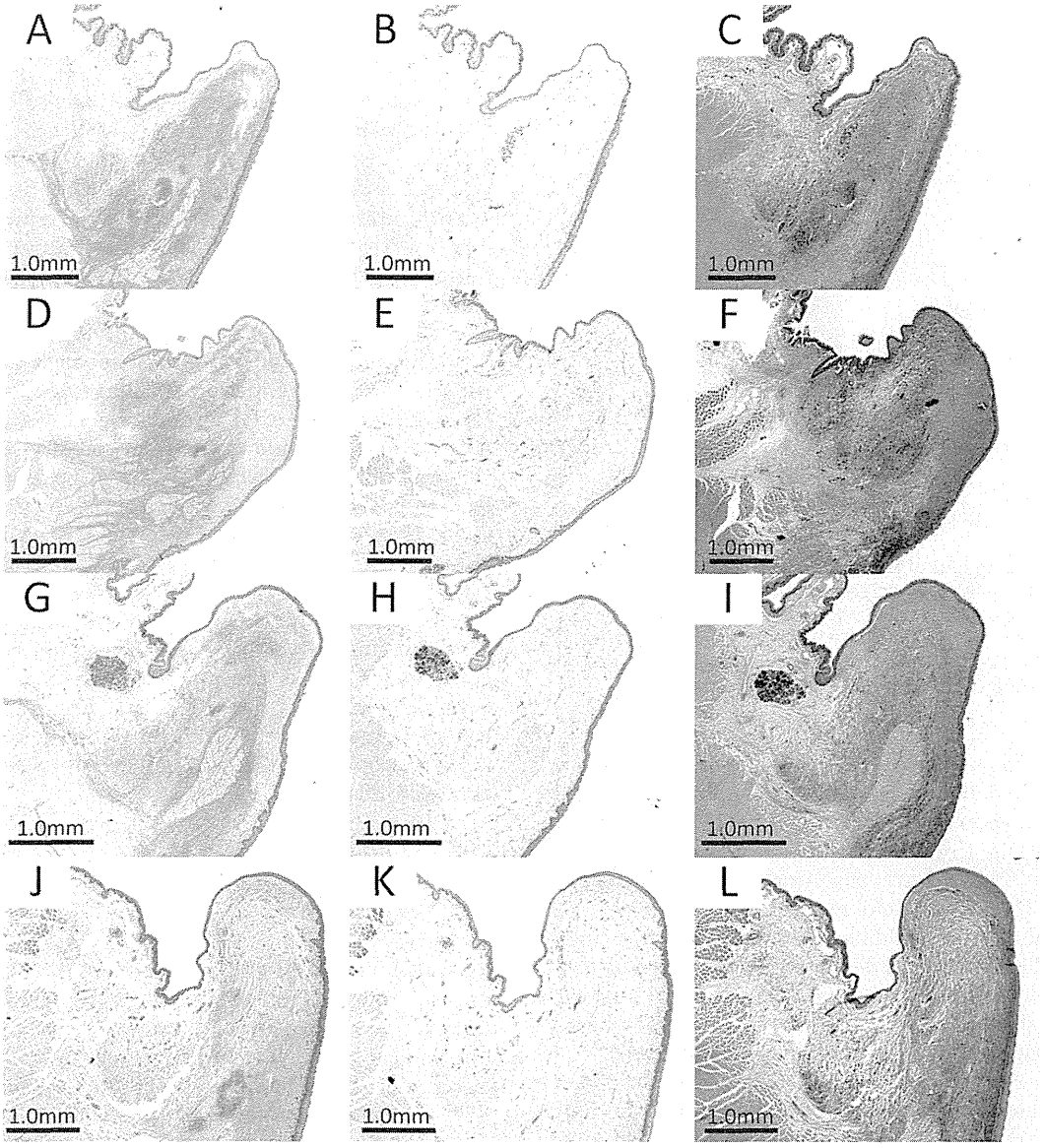

Fig. 4. Histological findings (coronal sections of vocal folds). Alcian blue staining without hyaluronidase digestion (A, D, G, J) and with hyaluronidase digestion (B, E, H, K), and Elastica van Gieson staining (C, F, I, L) of the normal group (A, B, C), the sham-treated group (D, E, F), the full hepatocyte growth factor (HGF)-treated group (G, H, I), and the 5 amino acid-deleted type HGF (dHGF)-treated group (J, K, L). The full HGF-treated group and the dHGF-treated group showed restoration of hyaluronic acid compared to the sham-treated group. Collagen deposition (purple in Elastica van Gieson staining) of the full HGF-treated group and the dHGF-treated group was minimal compared to the sham-treated group. [Color figure can be viewed in the online issue, which is available at wileyonlinelibrary.com.]

Both the full HGF group and the dHGF group showed significantly lower PTP (Fig. 3A) and a higher ratio of NMWA (Fig. 3B) than the sham group. The full HGF group showed significantly smaller NGG (Fig. 3C) than the sham group. No significant differences were observed for each parameter between the full HGF group and the dHGF group.

Histological Examination

Alcian blue staining and the hyaluronidase digestion technique (Fig. 4) showed that deposition of HA in sham-treated vocal folds was reduced compared to the normal folds. Both the full HGF group and the dHGF group showed better restoration of HA, which resembled normal folds, than the sham-treated folds, although no significant difference was observed for the ratio of HA among the three groups (Fig. 5). The results also indicated better recovery of HA in the dHGF group than the full HGF group, although the difference did not reach statistical significance.

Elastica van Gieson staining showed that collagen deposition in both the full HGF group and the dHGF group was minimal compared to the sham group.

DISCUSSION

Human HGF has two natural forms: full-length HGF and dHGF. Nucleotide sequence analysis of cDNA clones for human HGF has demonstrated that HGF

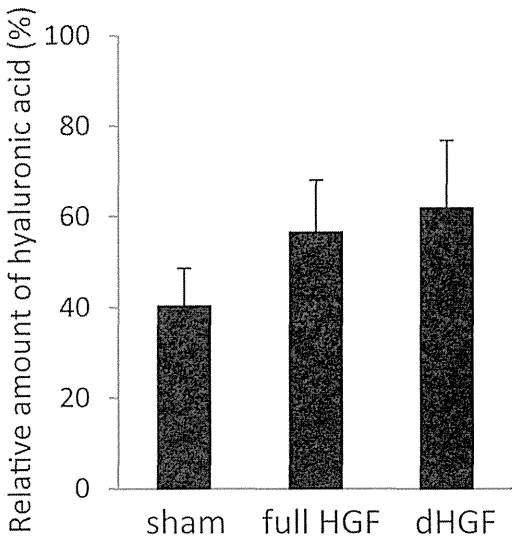

Fig. 5. The relative amount of hyaluronic acid. No significant difference was observed in the relative amount of hyaluronic acid among the three groups, although there was a tendency that the 5 amino acid-deleted type HGF (dHGF)-treated group showed a higher amount of HA compared to the sham-treated group and the full hepatocyte growth factor (HGF)-treated group.

consists of six major domains including a hairpin region and four kringle domains in the alpha chain, and a serine protease-like domain in the beta chain. dHGF lacks 5 amino acids in the first kringle domain compared to full-length HGF.[7,9,10] We have confirmed the regenerative effects of HGF on vocal fold mucosa in several animal studies including rats, rabbits, and canines using full-length HGF. These findings demonstrate the regenerative effects of full-length HGF on vocal fold scars and suggest that clinical trials are warranted, but this has been hampered by the lack of GMP-compatible full-length HGF.

Recently, recombinant human dHGF was produced by Chinese hamster ovary cells transfected with human dHGF cDNA under a GMP procedure. It has been suggested that the deletion of five amino acids in the first kringle domain might affect the biological activity of HGF.[10] However, it was reported that dHGF had higher mitogenic activity than full HGF for rat hepatocytes.[10,22] Furthermore, Shima et al.[10] investigated the differences between the biological activities of full HGF and dHGF in an in vitro study and reported that dHGF was more potent than full HGF for the stimulation of DNA synthesis in epithelial cells, whereas full HGF was more potent than dHGF in the stimulation of DNA in mesenchymal cells. However, it is widely recognized that both full HGF and dHGF have similar biological activities. Most experimental animal studies that examine the therapeutic effects of HGF in various diseases have been conducted using recombinant human dHGF. Moreover, clinical trials of recombinant HGF for the treatment of kidney disease and amyotrophic lateral sclerosis are currently in process using recombinant dHGF. Considering the advantage of the existence of a GMP-compatible product, we anticipate the clinical application of dHGF for the treatment of vocal fold scars.

The current study indicates a comparable activity of dHGF as full HGF. A dHGF injection to scarred vocal folds resulted in improvement of PTP, mucosal wave, and glottis competence. PTP is a marker that indicates the viscoelasticity of the tissues, because stiffer tissues require more pressure to be vibrated. Reduction of PTP means restoration of pliability of the mucosa. Consequently, the mucosal wave amplitude tended to become larger with complete glottic closure, which is similar to normal vocal fold vibrations. Only the dHGF group showed a statistically significant difference in glottic closure (NGG) as compared to the sham group.

The histological examinations demonstrated restoration of HA and reduction of collagen deposition in both the dHGF and full HGF groups. Because HA is regarded as a critical molecule to maintain ideal viscoelasticity of the vocal folds, restoration of HA is thought to be important to recover mucosal vibratory potency. There was a trend that dHGF induced more HA deposition as compared to full HGF, although there was no significant difference between the two HGFs, probably because of the small number of animals used in this study.

The current results are encouraging because dHGF generated at least the same power of regeneration of vocal fold scars as full HGF. dHGF shows promise for use in human clinical trials in patients with vocal fold scars using the GMP product currently used in other clinical trials.

CONCLUSION

dHGF showed a comparable potential for regenerative effects on vocal fold scarring as full HGF in terms of improvement of phonation threshold pressure, mucosal wave amplitude, glottis competency, as well as at the histological level. It is highly desirable to confirm the efficacy of dHGF as a GMP product in human clinical trials for patients with vocal fold scars.

BIBLIOGRAPHY

1. Hirano S. Current treatment of vocal fold scarring. *Curr Opin Otolaryngol Head Neck Surg* 2005;13:143–147.
2. Rousseau B, Hirano S, Scheidt TD, et al. Characterization of vocal fold scarring in a canine model. *Laryngoscope* 2003;113:620–627.
3. Hirano S, Bless DM, Rousseau B, Welham N, Scheidt T, Ford CN. Fibronectin and adhesion molecules on canine scarred vocal folds. *Laryngoscope* 2003;113:966–972.
4. Thibeault SL, Rousseau B, Welham NV, Hirano S, Bless DM. Hyaluronan levels in acute vocal fold scar. *Laryngoscope* 2004;114:760–764.
5. Rousseau B, Hirano S, Chan RW, et al. Characterization of chronic vocal fold scarring in a rabbit model. *J Voice* 2004;18:116–124.
6. Hirano S, Minamiguchi S, Yamashita M, Ohno T, Kanemaru S, Kitamura M. Histologic characterization of human scarred vocal folds. *J Voice* 2009;23:399–407.
7. Matsumoto K, Nakamura T. Hepatocyte growth factor (HGF) as a tissue organizer for organogenesis and regeneration. *Biochem Biophys Res Commun* 1997;239:639–644.
8. Nakamura T, Nawa K, Ichihara A, Kaise N, Nishino T. Purification and subunit structure of hepatocyte growth factor from rat platelets. *FEBS Lett* 1987;224:311–316.
9. Mizuno S, Kurosawa T, Matsumoto K, Mizuno-Horikawa Y, Okamoto M, Nakamura T. Hepatocyte growth factor prevents renal fibrosis and dysfunction in a mouse model of chronic renal disease. *J Clin Invest* 1998; 101:1827–1834.
10. Shima N, Tsuda E, Goto M, et al. Hepatocyte growth factor and its variant with a deletion of five amino acids are distinguishable in their biological activity and tertiary structure. *Biochem Biophys Res Commun* 1994;200: 808–815.

11. Hirano S, Bless D, Heisey D, Ford C. Roles of hepatocyte growth factor and transforming growth factor beta1 in production of extracellular matrix by canine vocal fold fibroblasts. *Laryngoscope* 2003;113:144–148.
12. Hirano S, Bless DM, Massey RJ, Hartig GK, Ford CN. Morphological and functional changes of human vocal fold fibroblasts with hepatocyte growth factor. *Ann Otol Rhinol Laryngol* 2003;112:1026–1033.
13. Hirano S, Bless DM, Heisey D, Ford CN. Effect of growth factors on hyaluronan production by canine vocal fold fibroblasts. *Ann Otol Rhinol Laryngol* 2003;112:617–624.
14. Ohno T, Hirano S, Kanemaru S, et al. Expression of extracellular matrix proteins in the vocal folds and bone marrow derived stromal cells of rats. *Eur Arch Otorhinolaryngol* 2008;265:669–674.
15. Kishimoto Y, Hirano S, Suehiro A, et al. Effect of exogenous hepatocyte growth factor on vocal fold fibroblasts. *Ann Otol Rhinol Laryngol* 2009; 118:606–611.
16. Suehiro A, Wright H, Rousseau B. Optimal concentration of hepatocyte growth factor for treatment of the aged rat vocal fold. *Laryngoscope* 2011;121:1726–1734.
17. Hirano S, Bless DM, Nagai H, et al. Growth factor therapy for vocal fold scarring in a canine model. *Ann Otol Rhinol Laryngol* 2004;113:777–785.
18. Hirano S, Bless DM, Rousseau B, et al. Prevention of vocal fold scarring by topical injection of hepatocyte growth factor in a rabbit model. *Laryngoscope* 2004;114:548–556.
19. Ohno T, Hirano S, Kanemaru S, et al. Drug delivery system of hepatocyte growth factor for the treatment of vocal fold scarring in a canine model. *Ann Otol Rhinol Laryngol* 2007;116:762–769.
20. Kishimoto Y, Hirano S, Kitani Y, et al. Chronic vocal fold scar restoration with hepatocyte growth factor hydrogel. *Laryngoscope* 2010;120:108–113.
21. Gray SD, Titze IR, Chan R, Hammond TH. Vocal fold proteoglycans and their influence on biomechanics. *Laryngoscope* 1999;109:845–854.
22. Matsumoto K, Takehara T, Inoue H, Hagiya M, Shimizu S, Nakamura T. Deletion of kringle domains or the N-terminal hairpin structure in hepatocyte growth factor results in marked decreases in related biological activities. *Biochem Biophys Res Commun* 1991;181:691–699.

分子標的薬・コンパニオン診断薬の医療技術評価の現状と課題

Health Technology Assessment(HTA)of molecular targeted drugs and companion diagnostics

村田京子　川上浩司
Kyoko MURATA and Koji KAWAKAMI
京都大学大学院医学研究科薬剤疫学

◎分子標的薬の開発が進むとともに，今後ますます個別化医療は加速し，薬剤は有効な集団にのみ与えられるようになっていくであろう．分子標的薬の開発とともに，この“有効な集団”を絞り込むためにコンパニオン診断薬も開発される．昨今，分子標的薬およびコンパニオン診断薬の医療技術評価(HTA)についての議論が行われている．HTAは医療技術を医学的・社会的・倫理的・経済的な観点などから総合的に検討するものであり，評価の結果は新薬や新技術などの保険償還の可否や償還価格の設定，臨床ガイドラインの策定などへの使用が期待されている．日本では分子標的薬・コンパニオン診断薬のHTAはまだほとんど行われていないが，医療保険制度の枠組みのなかで，このような医療を効率的に提供していくためにはHTAが不可欠であり，その適用範囲や社会の受容といった種々の課題に対して幅広い議論が求められる．

Key word：分子標的薬，コンパニオン診断薬，医療技術評価(HTA)

日本では国民皆保険による公的医療保険制度が構築されていることから，効率的な医療を提供することが求められる．個別化医療は，より安全で有効な先端技術の利用，医療の質の向上やむだの削減のために重要視されている[1]．分子標的薬の開発が進むとともに，今後ますます個別化医療は加速し，薬剤は有効な集団にのみ与えられるようになっていくであろう．分子標的薬の開発とともに，この“有効な集団”を絞り込むためにコンパニオン診断薬も開発される．

昨今，分子標的薬およびコンパニオン診断薬の医療技術評価(health technology assessment：HTA)についての議論が活発に行われるようになってきており，本稿ではわが国における現状と課題を中心に概説する．

医療技術評価(HTA)

HTAは，エビデンスに基づく医療(evidence based medicine：EBM)や比較効果研究(comparative effectiveness research：CER)より一歩進んだ概念であり，“その治療は効果があるのか”“何がもっとも効果的に機能するのか”に加えて，“その治療を受ける価値があるのか”という問いにまで答えようとするものである[2]．つまり医療技術を医学的な観点だけではなく，社会的・倫理的・経済的な観点などから総合的に評価するものである[3]．

その評価手法は疫学，生物統計学，行動科学といったソリッドな科学に基づいており，1990年代後半からヨーロッパ，アメリカ，アジア諸国においてHTAを実践する独立機関が設立されている．これらの国では，HTAの結果は新薬や新技術などの保険償還の可否や償還価格の設定，臨床

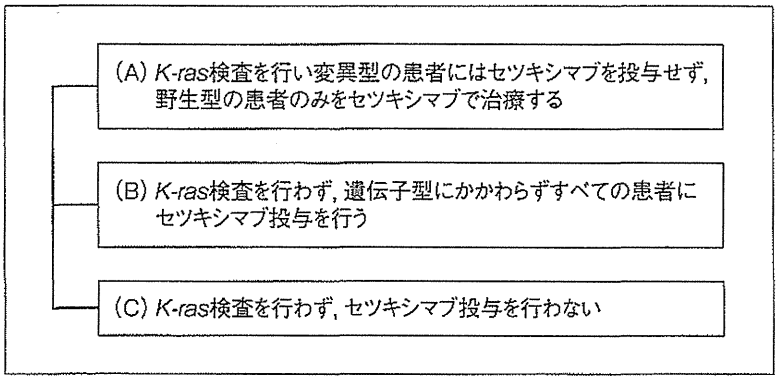

図 1　白岩らの研究で用いられた比較対照群

ガイドラインの策定などに用いられている．日本においては，国民医療費が増加しつづけているという状況のなか，2012 年 5 月に厚生労働省の諮問機関である中央社会保険医療協議会に費用対効果評価専門部会が設置され，医療技術の保険適用などの決定に費用対効果の観点を導入することについての議論が開始された[4]．

コンパニオン診断薬においては，2011 年 10 月に社団法人日本臨床検査薬協会，米国医療機器・IVD 工業会および欧州ビジネス協会が，内閣官房の医療イノベーション推進室，厚生労働省および独立行政法人医薬品医療機器総合機構に向けて“個別化医療を推進するためのコンパニオン診断薬のインフラ整備に関する提案書”を発出し，検査の技術革新や製品開発へのインセンティブを加算した保険点数付与の仕組みの導入や，コンパニオン診断薬の医療経済的な価値を反映した保険点数の付与を要望している[5]．

診療報酬上のコンパニオン診断薬の価値

コンパニオン診断薬を含む体外診断薬の診療報酬は検査の実施料と判断料からなり，その保険点数には検査キット代だけではなく，測定にかかる人件費や検体前処理，輸送，報告など，検査にかかるすべてのプロセスに対する費用が含まれている[6]．これまで，遺伝子検査の診療報酬は 2,000 点が上限と考えられており，その技術や臨床的有用性を反映した償還価格の付与が行われがたい仕組みであった[5]．2010 年 4 月に 2,000 点で保険収載がなされた *K-ras* 遺伝子検査キットについては，保険収載後，8,000 点に設定したとしても費用対効果が優れるという研究結果が示されたが[7]，2012 年度診療報酬改定ではわずかな増点(2,100 点)にとどまった．

一方，2012 年 3 月に承認されたコンパニオン診断薬については従来の遺伝子検査などの診療報酬である約 2,000 点を大きく上まわり，非小細胞肺癌に対する *ALK* 融合遺伝子標本作製(fluorescent *in situ* hybridization：FISH 法)には 6,520 点，再発または難治性の成人 T 細胞白血病リンパ腫に対する CCR4 蛋白の検出(免疫組織化学染色法および flow cytometry 法)には 10,000 点という点数が付けられており[8,9]，今後はコンパニオン診断薬に診療報酬上で高い価値が与えられる事例が増えると予想される．しかし，これまで実施されていなかった新技術の革新性を適切に評価することは難しい．また，市場ニーズが低いが臨床的に価値が高い場合においても，コンパニオン診断薬の適切な償還価格を算出することはきわめて難しい[10]．

分子標的薬・コンパニオン診断薬の経済評価

ヨーロッパにおいて HTA はさまざまな医薬品に適用されてきたが，コンパニオン診断薬を含む診断薬ではほとんど実施されていない[11]．このようななか，2013 年 8 月に HTA が進んでいるイギリスにおいて，HTA を所管する行政機関である National Institute for Health and Care Excellence(NICE)が，費用対効果が優れていると評価することができないとして，*ALK* 融合遺伝子陽性の非小細胞肺癌の治療に ALK 阻害薬であるクリゾチニブの使用を推奨しないとするガイダンス[12]を公表し，衝撃を与えた．

日本でも分子標的薬・コンパニオン診断薬のHTAはほとんど行われていないが，白岩らが実施した大腸直腸癌治療での*K-ras*遺伝子検査を使用したセツキシマブの経済評価では[7,13]，おもな結果として図1の(A)と(B)の比較から，*K-ras*遺伝子検査を行うことにより約50万円/人の費用削減効果があり，効果も点推定値として*K-ras*遺伝子検査を実施するほうが高く，費用対効果としてdominant(優位)であることが示された．したがって，セツキシマブを使用するのであれば*K-ras*遺伝子検査を実施すべきであるという結論を導いている．一方，セツキシマブを用いる治療自体については(A)と(C)の比較で，ICER(incremental cost-effectiveness ratio：増分費用対効果)は1,100万円/LYG(life years gained：獲得生存年)または1,600万円/QALY(quality adjusted life years：質調整生存年)であり，(B)と(C)の比較では1,400万円/LYGまたは2,100万円/QALYであり，費用対効果は優れるとは評価されなかった．また，革新的な新技術の価値を適切に評価するためにvalue-based pricingについても検討すべきであると述べられており，同様の指摘が他の研究や報告書にもみられる[14,15]．

倫理的・社会的な側面からの評価の必要性

コンパニオン診断薬による検査によって特定された“有効でない集団”は，当該治療を受ける機会を失ってしまう．日本のように等しく保険料を支払う国民/患者の立場からすれば，治療の選択肢が限られることや“有効な集団”のみが公的医療費で治療されるといった不平等な医療資源の配分に不満を抱く可能性がある．そこには検査特有の感度・特異度といった問題も内在する．さらに，上述したイギリスの例のように，費用対効果が優れていないため公的な保険償還がなされない可能性もある．分子標的薬やコンパニオン診断薬に限らず，そもそもHTAの主要な評価である費用対効果分析の結果は，つねに国民に受け入れられるものとはいいがたい．ある医療技術が費用対効果が優れないとして保険適用にならないことは，その使用によって症状の改善や治癒の可能性に懸けたいと望む患者にとって耐えがたいものである．また，コンパニオン診断薬による検査で，分子標的薬を使用できないと判断された場合，その検査代はだれが負担するのか，といった課題も生じる[14]．このような，倫理的・社会的な側面からも分子標的薬とコンパニオン診断薬の使用に際しては十分な評価や議論がなされ，国民の理解を得ておかなければならない．

おわりに

分子標的薬・コンパニオン診断薬に対しては費用対効果といった医療経済的な観点からだけではなく，多面的な観点でのHTAを実施すべきだと考えられる．日本の医療保険制度の枠組みのなかで，このような医療を効率的に提供するためにはHTAが不可欠であり，その適用範囲や社会の受容といった種々の課題に対して，今後幅広い議論を行っていくことが求められる．

文献/URL

1) 内閣官房医療イノベーション会議：医療イノベーション5カ年戦略．2012．(http://www.kantei.go.jp/jp/singi/iryou/5senryaku/)
2) Organisation for Economic Co-operation and Development：OECD Health Policy Studies-Value for Money in Health Spending. OECD Publishing, 2010.〔小林大高，坂巻弘之(訳)：OECD医療政策白書—費用対効果を考慮した質の高い医療をめざして．明石書店，2011.〕
3) 科学技術振興機構研究開発戦略センター ライフサイエンス・臨床医学ユニット：調査検討報告書—医療の持続的発展に向けた戦略的な医療技術評価(Health Technology Assessment)の推進．2012．(http://www.jst.go.jp/crds/pdf/2011/RR/CRDS-FY2011-RR-08.pdf)
4) 厚生労働省：中央社会保険医療協議会費用対効果評価専門部会．2012．(http://www.mhlw.go.jp/stf/shingi/2r98520000008ffd.html#shingi128159)
5) 日本臨床検査薬協会・他：個別化医療を推進するためのコンパニオン診断薬のインフラ整備に関する提案書．2011．(http://www.jacr.or.jp/osirase/shiryou/doc/111021teiansyo.pdf)
6) 林　邦彦：政策研ニュース，**34**：27-31，2011．
7) Shiroiwa, T. et al.：*Mol. Diagn. Ther.*, **14**：375-384, 2010.
8) 稲垣英仁，津谷喜一郎：がん分子標的治療，**10**：282-286，2012．
9) 厚生労働省：第222回中央社会保険医療協議会総会議事録．2012．(http://www.mhlw.go.jp/stf/shingi/2r98520000027xg8.html)
10) 田澤義明：臨床病理，**61**：435-442，2013．
11) 林　邦彦：政策研ニュース，**36**：9-14，2012．
12) National Institute for Health and Care Excellence：NICE technology appraisal guidance. TA296.

Crizotinib for previously treated non-small-cell lung cancer associated with an anaplastic lymphoma kinase fusion gene. 2013.(http://publications.nice.org.uk/crizotinib-for-previously-treated-non-small-cell-lung-cancer-associated-with-an-anaplastic-lymphoma-ta296/guidance)
13) 白岩　健・他：病理と臨床，**30**：1351-1354，2012.
14) Faulkner, E. et al.：*Value Health*, **15**：1162-1171, 2012.
15) Garau, M. et al.：*OHE*, Research Paper 12/03, 2012.

*　　*　　*